



Preparation and characterization of FeMoCoS nanocomposites for efficiently adsorbing dye from wastewater

Bai Sun^{a,c,*}, Angang Hu^a, Yunming Cheng^a, Haiyan Zhou^a, Xiaojie Song^b, Jie Mao^a, Yun Wang^a, Xiangxiang Wang^a, Shuguang Zhu^a, Xinli Cai^{a,*}

^aEngineering Research Center of Building Energy Efficiency Control and Evaluation of the Ministry of Education, College of Environment and Energy Engineering, Anhui Jianzhu University, Hefei 230601, China, emails: bsun@mail.ustc.edu.cn (B. Sun), ahcxl@163.com (X. Cai), 1332126924@qq.com (A. Hu), 502283466@qq.com (Y. Cheng), 1450771215@qq.com (H. Zhou), 17433503@qq.com (X. Song), 972536164@qq.com (J. Mao), 596820989@qq.com (Y. Wang), 350992818@qq.com (X. Wang), zhushuguang@ahjzu.edu.cn (S. Zhu)

^bSchool of Materials and Chemical Engineering, Anhui Jianzhu University, Hefei 230601, China

^cEnvironmental Materials and Pollution Control Laboratory, Hefei Institute of Physical Science, Chinese Academy of Sciences, Hefei 230031, China

Received 23 December 2021; Accepted 12 May 2022

ABSTRACT

In this study, FeMoCoS (FMCS) nanocomposites were designed and fabricated through a hydrothermal method as a new efficient adsorbent to remove organic dyes in wastewater. The morphology and microstructure of the adsorbent were characterized by using scanning electron microscopy, energy-dispersive X-ray spectroscopy, Brunauer–Emmett–Teller surface area and Fourier-transform infrared spectroscopy. The effects of adsorption isotherm, kinetics, initial concentration and pH value of Rhodamine B (RhB) solution on the experiment were also studied. The results show that FMCS has good adsorption capacity for RhB solution, and the maximum adsorption capacity is 280.89 mg/g calculated by using a Langmuir isotherm model. Column study was made to achieve bulk removal of the dye. Column adsorption capacity has been found to be greater than the batch adsorption capacity. Moreover, the maximum removal rate of RhB reaches 99.64% at pH = 7 and $\text{pH}_{\text{PZC}} = 9.57$ according to zeta potential. The adsorption kinetics match the pseudo-second-order model, indicating that the adsorption process is dominated by chemisorption. After 5-cycles of consecutive adsorption, the adsorbent can still maintain a high adsorption capacity, indicating a good potential for RhB removal from wastewater.

Keywords: FeMoCoS; Nanocomposites; Rhodamine B; Adsorption

1. Introduction

Scientific literatures show that the annual output of dyes is as high as 7×10^5 tons, and nearly 10%–15% of the dyes are directly released into the environment without being treated [1]. Chemical processes used in several industries, including paper, textiles, plastics, cosmetics, printing, involve dyes [2], which are often thrown away as untreated waste and mixed with water resources [3]. Dyes

are chemically stable and non-degradable [4]. Wastewater with dyes is characterized by complex composition, high concentration, large variation of water quality and quantity, strong pH, high organic matter content, high chroma and high toxicity [5]. In addition, some dyes and their degradation products cause skin irritation, eye burns, diarrhea, cancer and mutagenic or carcinogenic effects on living organisms including humans [6,7]. Rhodamine B (RhB) is a kind of high water-soluble red dye of xanthine. It is widely used

* Corresponding authors.

as a colorant in textiles and food, and is also a well-known water-tracer fluorescence agent [8]. Therefore, considering the harmful and harmful effects of RhB, it is worthwhile to systematically remove RhB with efficient adsorbents.

The common methods for purifying wastewater with dye include adsorption [9], biological [10], chemical oxidation [11], membrane separation [12], coagulation and flocculation [13], photocatalysis [14], etc. Among them, adsorption is one of the most effective methods to purify water contaminated by dissolved substances and drugs [15,16]. The adsorption process has no toxicity to water, which is why the removal of organic waste is superior to conventional treatment [17]. It has the advantages of simple operation, high efficiency and wide range of materials [18]. At present, the most commonly used adsorbents are activated carbon [19,20], clay [21], polymer materials [22] and metal-organic framework [23,24]. Even some waste materials can be used as potential adsorbents [25], such as black turmeric powder [26], papaya peel charcoal [27], *Chenopodium album* [28] and *Curcuma caesia* [29]. It is necessary to study an adsorbent that is environmentally friendly, cost-effective [23], simple production method and high efficiency for adsorption and degradation [30]. Transition metal (Fe, Co, Mo, etc.) oxides and sulfides have been widely reported due to their good adsorption properties in dye wastewater [31]. Because of its high catalytic activity [32], CoS has become the most optimistic class of efficient sorbents in recent years. The introduction of other non-noble metal elements into CoS can further improve the performance. Iron based nanoparticles are considered as a good adsorbent candidate because of its strong chemical stability [33]. Nanostructured FeMoCoS (FMCS) exhibits larger specific surface area [34], unique porous network, high synergy [35] and excellent catalytic activity [36,37]. It can be reasonably predicted that the synthesis of these four elements and the preparation of economical and efficient adsorbent will have a good potential for the adsorption of pollutants.

Here, FMCS nanocomposites are synthesized by a simple hydrothermal method. RhB which is widely existed in industrial wastewater is selected to simulate xanthine contamination. The adsorption isotherms and adsorption kinetics are also studied. The samples are characterized by using scanning electron microscopy (SEM), Brunauer–Emmett–Teller (BET) surface area, energy-dispersive X-ray spectroscopy (EDS) and Fourier-transform infrared spectroscopy (FTIR), while the influence of pH values is investigated. In addition, the adsorption mechanism of the material has also been discussed.

2. Materials and methods

2.1. Reagents and instruments

The reagents used in the experiment mainly include iron nitrate ($\text{Fe}(\text{NO}_3)_3 \cdot 9\text{H}_2\text{O}$), cobalt nitrate ($\text{Co}(\text{NO}_3)_2 \cdot 6\text{H}_2\text{O}$), sodium molybdate ($\text{Na}_2\text{MoO}_4 \cdot 2\text{H}_2\text{O}$), thioacetamide ($\text{C}_2\text{H}_5\text{NS}$) and acetic acid ($\text{C}_2\text{H}_4\text{O}_2$) were purchased from Sinopharm Chemical Reagent Co., Ltd., (Shanghai, China) and used as received without further purification. Deionized water is prepared by FST-TOP-A24 superpure water equipment by Shanghai Fushite Instrument Equipment Co., Ltd., (China).

Scanning electron microscopy was performed on Zeiss Auriga microscope. EDS was performed on a Zeiss Auriga microscope equipped with an Oxford Inca X-Max 50 detector. BET surface area was measured (Micromeritics Co., USA). The Fourier transform infrared (FT-IR) spectra of the adsorbents before and after adsorption were recorded with a NEXUS-870 FT-IR spectrometer in the range of $4,000\text{--}400\text{ cm}^{-1}$. The wavelength change of the adsorbent was recorded in the range of $190\text{--}900\text{ cm}^{-1}$ using a UV-2600i UV-Vis spectrophotometer (Shimadzu Manufacturing Co., Ltd., China).

2.2. Fabrication of adsorbent

FMCS nanocomposites were synthesized by a hydrothermal method [38]. Firstly, 0.5 mmol $\text{Fe}(\text{NO}_3)_3 \cdot 9\text{H}_2\text{O}$, 1 mmol $\text{Co}(\text{NO}_3)_2 \cdot 6\text{H}_2\text{O}$, 1 mmol $\text{Na}_2\text{MoO}_4 \cdot 2\text{H}_2\text{O}$ and 1 mmol $\text{C}_2\text{H}_5\text{NS}$ were dissolved in 20 mL deionized water. Afterwards, 0.5 mL $\text{C}_2\text{H}_4\text{O}_2$ solution was added and stirred for 2 h. Secondly, the reaction mixture was transferred to a 100 mL Teflon lined stainless steel reaction kettle. The reaction kettle was placed in a constant temperature heating box and heated at 180°C for 12 h. Finally, the typical product of FMCS nanocomposites were then washed several times alternately with deionized water and anhydrous ethanol, and finally freeze-dried and ground for sieving.

2.3. Batch adsorption experiments

Different concentrations of RhB solution were used to simulate untreated dye wastewater. Batch adsorption experiments were carried out by adding 20 mg FMCS nanocomposites into 200 mL and 20 mg/L RhB solution. The whole experiment was carried out in a constant temperature oscillation chamber with shading, with the room temperature set at 25°C and the rotation speed at 150 rpm. After waiting for adsorption equilibrium, take a certain amount of supernatant, measure the absorbance value at the absorption wavelength of 554 nm with UV-Vis, calculate and analyze the results through the adsorption capacity formula. The effects of initial pH of RhB solution and adsorbent recycling on the experiment were studied by the same experimental method, and its kinetics and isotherms were studied.

2.4. Column study

A glass column having 20 cm length and 0.5 cm internal diameter was packed with 0.20 g of FMCS over a support of cotton wool, to perform the column operation. The length and cross section area of column bed was 0.5 cm and 0.2 cm^2 , respectively. Through this fixed bed, aqueous solution of RhB dye was allowed to run in a down flow motion with a flow rate of 2 mL/min. After each 5 min time interval 10 mL aqueous effluent samples were collected. The dye concentration was determined by measuring characteristics absorbance of the dye.

The breakthrough curve [39] is plotted in terms of C_t/C_0 vs. time, where C_t is the concentration of effluent at time t and C_0 is the initial concentration influent dye solution. The volume of effluent, V_{ef} can be calculated by using the following formula.

$$V_{ef} = vt \quad (1)$$

where t (min) is the flow time, and v (mL/min) is the flow rate.

Q_{total} (mg) is the amount of dye adsorbed at time t , and it can be obtained from the area under the breakthrough curve. The area under breakthrough curve can be calculated by the integration (determined using software OriginPro8).

$$Q_{total} = v \int_{t=0}^{t=t} (C_0 - C_t) dt \quad (2)$$

The total amount of dye (m_{total}) sent to the column at time t can be calculated by:

$$m_{total} = C_0 vt \quad (3)$$

The percentage removal of dye $R(\%)$ can be calculated as:

$$R = \frac{Q_{total}}{m_{total}} \times 100 \quad (4)$$

The column adsorption capacity of the adsorbent q_t (mg/g) at time t can be determined by the following equation (determined using software OriginPro8).

$$q_t = \frac{v \int_{t=0}^{t=t} (C_0 - C_t) dt}{m} \quad (5)$$

where m (g) is the amount of adsorbent used in column as fixed-bed.

3. Results and discussion

3.1. Sample characterization

SEM contains information about the surface morphology and composition of the sample, and the image of the synthetic sample shows particle size and high pore structure [40]. Fig. 1 shows the SEM images of FMCS nanocomposites before and after adsorption. It can be seen from Fig. 1a and b that the material has spherical micromorphology before adsorption, with close adjacent, loose and porous materials and uneven depressions on the surface. Fig. 1c and d show the material after adsorption, indicating that the size does not change significantly. The depression on the surface before adsorption disappears, and the material presents a three-dimensional shape.

BET surface area analysis was used to determine the physicochemical characteristics of the FMCS. Fig. 2a displays the N_2 adsorption–desorption isotherm of FMCS. The adsorption isotherm belongs to type IV curve. A clear hysteresis line appears between P/P_0 and 0.6–1.0, which is caused by capillary condensation. The BET method (Fig. 2b) was used to determine the specific surface area and pore diameter of the FMCS, which is 24.8728 m^2/g and 27.2805 nm respectively, indicating that the pore size of FMCS are mainly mesopores. The pore-volume of FMCS is 0.1693 cm^3/g .

The EDS spectrum of FMCS nanocomposites is shown in Fig. 3. The results show that the composite contains iron, molybdenum, cobalt, and sulfur elements that all elements are evenly distributed in the composite materials.

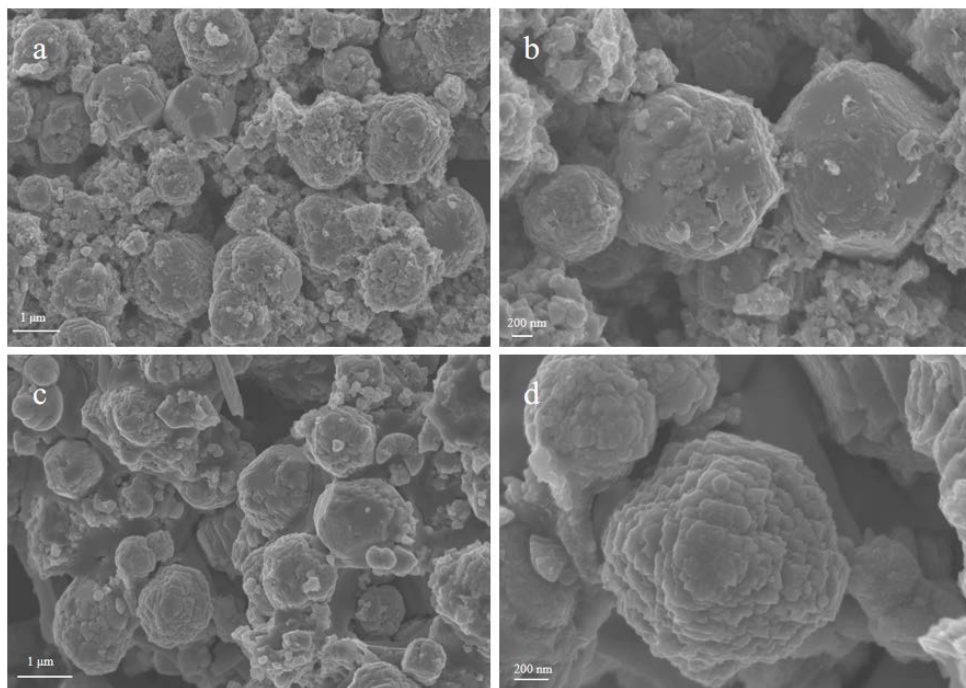


Fig. 1. SEM images of FMCS nanocomposites, (a,b) before adsorption, (c,d) after adsorption.

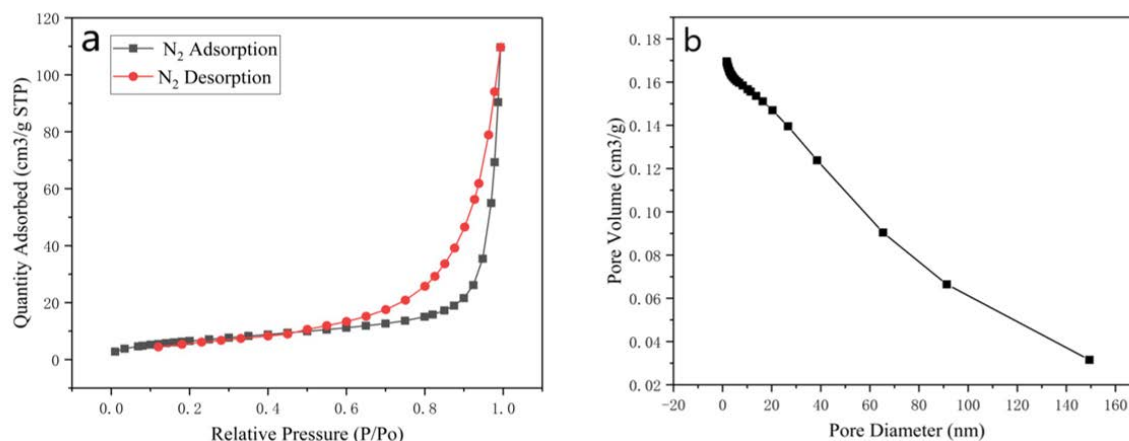


Fig. 2. (a) N₂ adsorption–desorption isotherms and (b) pore diameter distribution of FMCS.

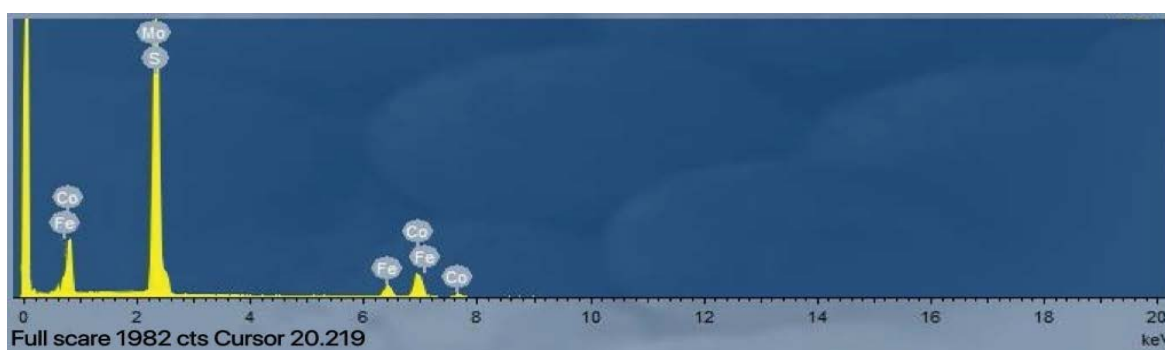


Fig. 3. EDS spectrum of FMCS nanocomposites.

The content of molybdenum in the sample is small, indicating that the molybdenum compound would not form a fixed crystal form.

3.2. Adsorption isotherm models and thermodynamics

Freundlich and Langmuir models were used to investigate the mechanism of the adsorption and to calculate the adsorption capacity [41]. Freundlich and Langmuir models and linear equations were used to study the adsorption performance of FMCS. Eqs. (6) and (7) are usually used to fit experimental results [42,43]. The corresponding parameters of the two models are shown in Table 2. Thermodynamic parameters can be obtained from Eqs. (8) and (9) [44,45].

$$\frac{C_e}{q_e} = \frac{C_e}{q_m} + \frac{1}{K_L \times q_m} \tag{6}$$

$$\ln q_e = \frac{1}{n} \ln C_e + \ln K_F \tag{7}$$

$$\Delta G = -RT \ln K \tag{8}$$

$$\ln K = \frac{-\Delta H}{RT} + \frac{\Delta S}{R} \tag{9}$$

where C_e (mg/L) is the concentration after equilibrium adsorption; q_e (mg/g) is the adsorption capacity after equilibrium; q_m (mg/g) and K_L (L/mg) are the maximum adsorption capacity and constants calculated by Langmuir equation. K_F (mg/g), n is the adsorption constant of Freundlich equation. R is the general gas constant (8.314 J/(mol/K)), T is the temperature (K); K is the Langmuir adsorption constant of; ΔS is the entropy change; ΔG is the Gibbs free energy change; ΔH is the enthalpy change.

Langmuir and Freundlich isothermal models were used to analyze the adsorption equilibrium. The adsorption results fitted by the models at different temperatures are shown in Fig. 4 and Table 1. It can be seen from Fig. 4b and c that the maximum R^2 of Langmuir model at different temperatures is 0.997, which is greater than the correlation coefficient R^2 of Freundlich isotherm model, indicating that Langmuir isotherm model can better describe the adsorption process. The results indicate that FMCS nanocomposites carry out monolayer adsorption and the adsorption sites on the adsorbent are evenly distributed. The Langmuir isotherm model shows that the maximum adsorption capacity of FMCS nanocomposites can reach 280.89 mg/g. By comparing the adsorption capacity of different adsorbents in Table 3, it can be concluded that FMCS nanocomposites have higher adsorption capacity for RhB compared with other adsorbents.

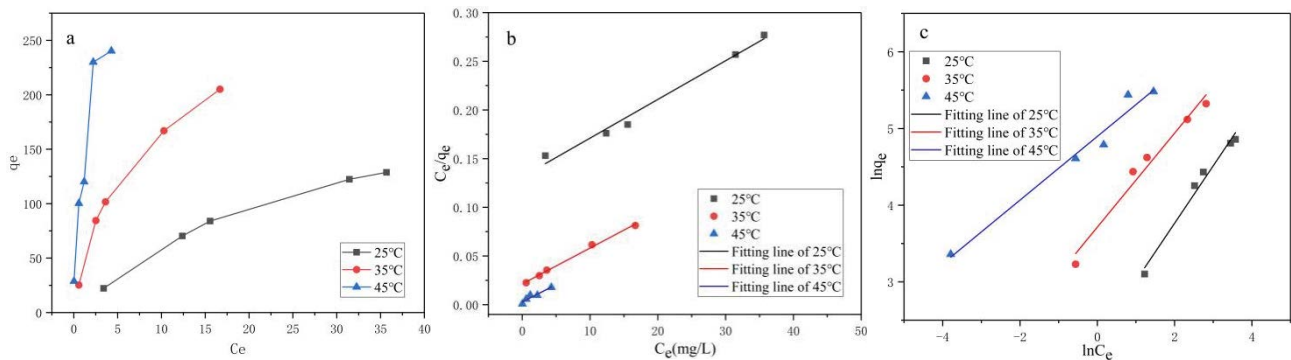


Fig. 4. Adsorption thermodynamics of (a) RhB at different temperatures; The fitting plot of (b) Langmuir model and (c) Freundlich model at different temperatures.

Table 1

Values of various adsorption isotherm constants for the uptake of RhB at different temperatures

Isotherm model	Langmuir $\left(\frac{C_e}{q_e} = \frac{C_e}{q_m} + \frac{1}{K_L q_m} \right)$			Freundlich $\left(\ln q_e = \frac{1}{n} \ln C_e + \ln K_F \right)$		
Parameters	(L/mg)	q_m (mg/g)	R^2	n	K_f (mg/g)	R^2
25°C	0.0303	251.25	0.992	1.3344	9.63	0.99
35°C	0.1722	271.73	0.997	1.6311	40.98	0.986
45°C	1.2447	280.89	0.954	2.4090	133.78	0.963

Table 2

Adsorption thermodynamic parameters

Samples	T (K)	ΔG (kJ/mol)	ΔS (kJ/K mol)	ΔH (kJ/mol)
	298	-4.65		
FMCS	308	-8.54	111.41	15.98
	318	-10.64		

Thermodynamic analysis of adsorption is a necessary condition for correctly understanding and predicting adsorption mechanism. Fig. 4a shows that at the same temperature, the equilibrium adsorption capacity of RhB increases with the increase of equilibrium concentration. At the same equilibrium concentration, the equilibrium adsorption capacity increases with the increase of temperature, indicating that the adsorption performance of FMCS improves with the increase of temperature. According to the data in Table 1, the parameters can be calculated as shown in Table 2. The adsorption of RhB by FMCS is a spontaneous endothermic reaction, because of the $\Delta G < 0$, $\Delta S > 0$ and $\Delta H > 0$.

3.3. Kinetic study

Adsorption kinetics describes the relationship between adsorption rate and efficiency. In order to further analyze the adsorption kinetics, linear and nonlinear adsorption kinetic models are used to describe the experimental data. The use of nonlinear models is to reduce the error caused by the conversion of nonlinear models to linear models [56,57].

Table 3

Comparison of adsorption capacity of different adsorbents

Adsorbents	Adsorption capacity (mg/g)	Reference
sAC	35.7	[46]
M3-OBDCa	50.32	[47]
MTV-MOFs	156	[48]
TMPTA-G-M	45.64	[49]
NiO/SiO ₂ nanocomposites	68	[50]
MIL-125(Ti)	180	[51]
Co ₃ O ₄ @g-C ₃ N ₄	100	[52]
Z-scheme CeO ₂ @LDH	57.85	[53]
E-spun GO/MIL-101(Fe)/PANCMa NFs	10.46	[54]
Rice husk	42.06	[55]
FMCS	280.89	This work

Linear form of pseudo-first-order:

$$\log(q_e - q_t) = \log q_e - \frac{k_1 t}{2.303} \quad (10)$$

Linear form of pseudo-second-order:

$$\frac{t}{q_t} = \frac{1}{k_2 q_e^2} + \frac{t}{q_e} \quad (11)$$

where q_e (mg/g) and q_t (mg/g) are the adsorption capacity of RhB at equilibrium and at any time, respectively; t (min) is the adsorption time. k_1 (min^{-1}) is the rate constant of quasi-first-order dynamics. k_2 ($\text{g}/(\text{mg min})$) is the rate constant of pseudo-second-order dynamics.

In order to better understand the adsorption behavior of RhB on adsorbent, the effect of contact time by FMCS was studied. As shown in Fig. 5a, the adsorption capacity increases significantly, and then increases slowly with the extension of the contact time in the initial stage. The rapid adsorption of RhB at the beginning of the reaction is attributed to the existence of a large number of unoccupied adsorption sites on the adsorbent surface, which enables RhB to interact rapidly. When the active sites are gradually occupied, the adsorption process becomes slow and reaches equilibrium. In Fig. 5b, c and Table 4, when the initial concentration is 5 mg/L, the linear correlation coefficient R^2 of the pseudo-second-order kinetic equation is larger than that of the pseudo-first-order kinetic equation, indicating that the pseudo-second-order kinetic equation is suitable for describing the kinetic process. The good fitting with the pseudo-second-order model suggests the dominance of chemisorption.

3.4. Column adsorption study for removal of RhB

Fixed-bed column experiment has been carried out for comparison with batch technique for the removal of dye from wastewater. The RhB solution (80 mg/L) was allowed to pass through fixed-bed column at a flow rate of 2 mL/min. After 100 min, the effluent concentration reached to nearly 90% of the influent concentration, and the column started to get choked. Fig. 6 is obtained by plotting a graph between time of flow and C_t/C_0 . According to the integral area, the calculated adsorption capacity of FMCS for RhB is

30.35 mg/g. In Tables 4 and 5, the column adsorption capacity ($q_e = 30.35$ mg/g) is higher than the batch adsorption capacity ($q_e = 27.86$ mg/g).

3.5. Effect of pH on RhB adsorption

The pH value of the solution is an important factor affecting the adsorption process, which mainly affects the adsorption process by changing the surface charge and charge state of the adsorbent [58]. Corresponding adsorption experiments at different pH values from 3 to 12 are shown in Fig. 7a. It can be seen that the adsorbent has significant adsorption properties at all pH values. When the pH increases from 3 to 8, the removal rate of RhB remains at a high level. In order to understand

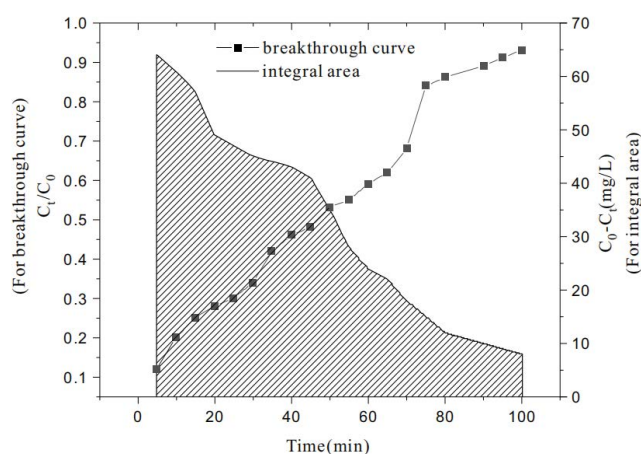


Fig. 6. Breakthrough curve and integral area of RhB on FMCS fixed-bed column.

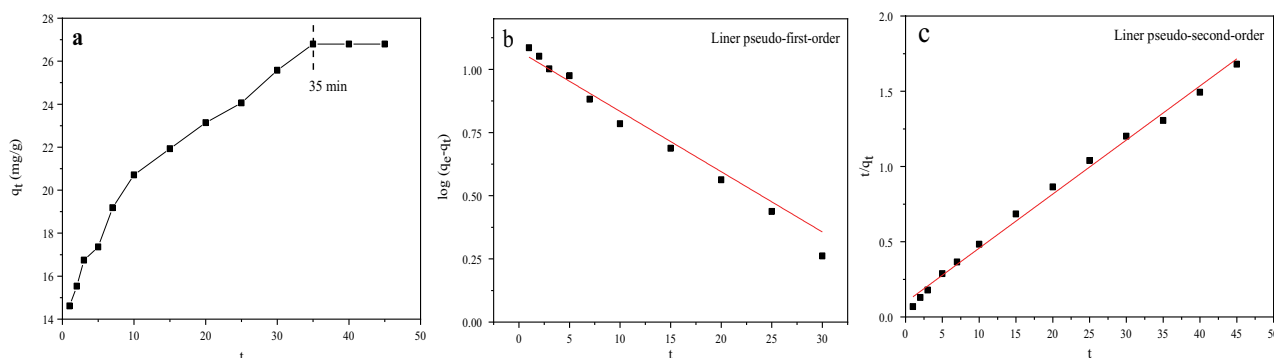


Fig. 5. (a) Kinetic experimental data of RhB adsorption by FMCS, (b) plot for the pseudo-first-order, and (c) plot for the pseudo-second-order.

Table 4
Pseudo-first and second-order kinetic parameters of RhB adsorption by FMCS

Kinetics model pseudo-first-order			Pseudo-second-order		
k_1 (min^{-1})	q_e (mg/g)	R^2	k_2 ($\text{g}/(\text{mg min})$)	q_e (mg/g)	R^2
0.0548	2.9218	0.9687	0.01319	27.86	0.9927

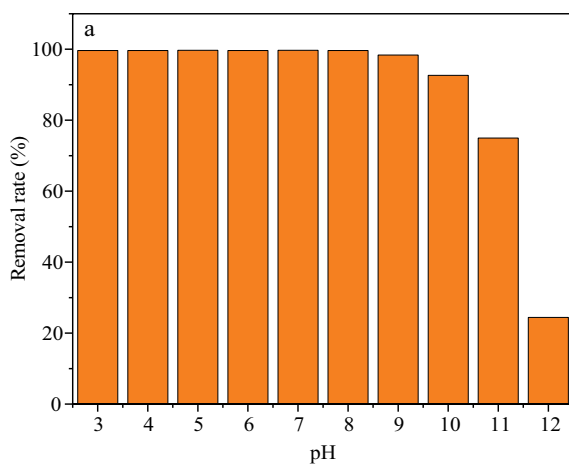
the mechanism behind these changes, zeta potentials of the adsorbents were measured, as shown in the Fig. 7b. According to the result of the zeta potential analysis of the adsorbent, the surface charge of the adsorbent is negative when $3 \leq \text{pH} \leq 8$, so there is a strong electrostatic attraction between the adsorbent and RhB. A high pH value is conducive for RhB adsorption due to the more obvious electrostatic attraction. When $\text{pH} = 7$, the removal rate of RhB is the highest, reaching 99.64%. For the higher alkaline pH ($9 \leq \text{pH} \leq 12$) values, the results differ and the adsorption of RhB decreases dramatically. It is explained by the fact that RhB exists in its zwitterion form at this range of pH, leading to the formation of dimers that aggregate along with a decrease of positive charge. Likewise, at high pH values beyond 9, the amount of the dyes adsorbed on the surface of the FMCS decreases. This may be due to the increasing number on Na^+ ions from the solution, which could compete with the cationic RhB in their basic forms for the equivalent active adsorption sites in the FMCS [48]. The zero point potentia (pH_{pzc}) is 9.57, when $\text{pH} < \text{pH}_{\text{pzc}}$. In addition, the positive charge increases when $\text{pH} > \text{pH}_{\text{pzc}}$.

3.6. Effect of recycling of FMCS on adsorption

The recyclability of adsorbent is important to evaluate the performance. The removal efficiency of RhB by FMCS for the first time reaches 96.38%. The same adsorption steps were continued after the eluent was used to treat the

Table 5
Breakthrough parameters for column adsorption study of RhB using FMCS

Flow rate (mL/min)	2
t (min)	100
Peak area (mg min/L)	3,035.89
q_e (mg/g)	30.35
m_{total} (mg)	16
Q_{total} (mg)	6.07
R (%)	37.94



adsorbent. The removal rate of RhB gradually decreases with the increase of the number of cycles. However, after five consecutive adsorption cycles, the removal rate of the adsorbent can still be maintained at 88.64%, indicating a good recyclability.

3.7. Adsorption mechanism

Fig. 8 shows the FTIR spectra of FMCS nanocomposite samples in the range of $4,000\text{--}500\text{ cm}^{-1}$. There is a close binding relationship between RhB adsorption and surface functional groups of FMCS. The surface properties of adsorbents are affected by the types and numbers of functional groups identified by FTIR. At $3,478\text{ cm}^{-1}$, the broadband band allocated to --NH_2 and --OH shifted right to $3,453\text{ cm}^{-1}$, with stronger peak intensity, indicating the adsorption of --NH_2 and --OH on FMCS [59]. The $1,677\text{--}1,636\text{ cm}^{-1}$ band is C--O stretching vibration in the carboxyl group, and all the carboxyl groups occur at very low intensity due to the high temperature generated in

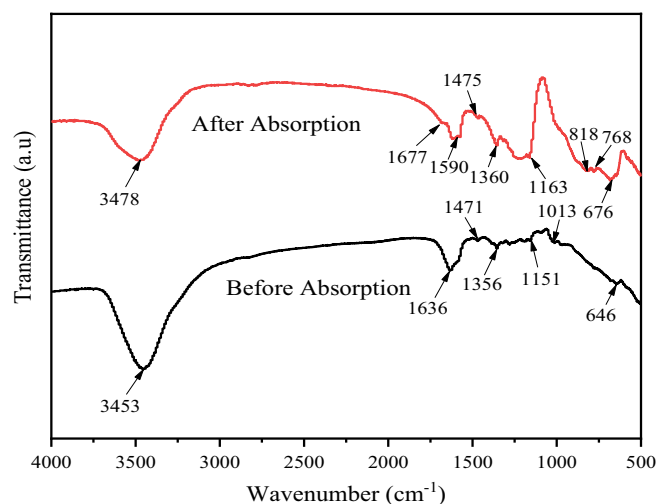


Fig. 8. FTIR spectra of FMCS nanocomposites before and after adsorption.

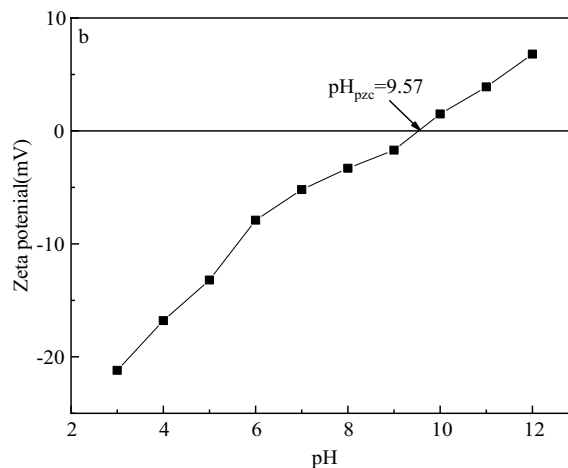


Fig. 7. (a) Effect of pH on RhB adsorption and (b) zeta potential dependent on the pH of adsorbent.

the combustion process [60]. In addition, due to humidity absorption, the low frequency band at $1,590\text{ cm}^{-1}$ can be considered as the bending vibrates between the H_2O layers [61]. The variation of adsorption from $1,475$ to $1,356\text{ cm}^{-1}$ is due to O–H bending, especially the O–H of phenol and COO^- of carboxyl groups [62]. The $1,163$ – $1,151\text{ cm}^{-1}$ band is attributed to C–O stretching vibration of different functional groups [63], such as esters, ethers, and phenol. The peaks near $1,013$ and 818 cm^{-1} reflect the stretching vibration of O=S=O and O–S–O in FMCS, respectively [64]. The peak at 718 cm^{-1} shows the stretching vibration of Mo–O [65]. In addition, a new absorption peak appears near 676 cm^{-1} , which belongs to Fe–O stretching vibration, and the stretching vibration of O–H and C=O bonds in FMCS is slightly enhanced, indicating that the surface polarity of FMCS is high, which is conducive to the adsorption of RhB [66].

4. Conclusion

In this paper, FMCS nanocomposites were synthesized through a hydrothermal method. The preparation process is simple. The results show that the adsorbent has a good adsorption performance for organic dye (RhB) in wastewater. According to the calculation of Langmuir isotherm model, the maximum adsorption capacity is 280.89 mg/g . The adsorption equilibrium is analyzed by Langmuir and Freundlich isotherm models. It can be seen that Langmuir isotherm model is better than Freundlich isotherm model in fitting experimental data. Thermodynamic parameters show that adsorption is a physical adsorption with spontaneous and endothermic characteristics. The column adsorption capacity is 30.35 mg/g , which is higher than the batch adsorption capacity. The pH_{pzc} is 9.57 , and the maximum removal rate reaches as high as 99.64% at $\text{pH} = 7$. In addition, the adsorbent has a good recyclability, which indicate a potential for applications.

Acknowledgments

The authors are especially grateful to the Project of National Key Research and Development Program (2019YFC0408503), the Natural Science Research Project of the Higher Education Institutions of Anhui Province (KJ2021A0616, KJ2020A0468), the National Natural Science Foundation of China (52103104, 61873003), the Natural Science Foundation of Anhui Province (1908085QE241), the first batch of natural science projects supported by surplus funds in 2021 of Anhui Jianzhu University (JZ202129, JZ202134) and the Scientific Research Start-up Foundation for Introduction of Talent, Anhui Jianzhu University (2016QD113).

References

- [1] X.M. Tian, Y.D. Song, Z.Q. Shen, Y.X. Zhou, K.J. Wang, X.G. Jin, Z.F. Han, T. Liu, A comprehensive review on toxic petrochemical wastewater pretreatment and advanced treatment, *J. Cleaner Prod.*, 245 (2020) 118692, doi: 10.1016/j.jclepro.2019.118692.
- [2] C. Arora, S. Soni, P.K. Bajpai, J. Mittal, A. Mariyam, Chapter 14 – Dye Removal From Waste Water Using Metal Organic Frameworks, *Management of Contaminants of Emerging Concern (CEC) in Environment*, 14 (2021) 375–394.
- [3] C. Arora, S. Soni, S. Sahu, J. Mittal, P. Kumar, P.K. Bajpai, Iron based metal organic framework for efficient removal of methylene blue dye from industrial waste, *J. Mol. Liq.*, 284 (2019) 343–352.
- [4] S. Soni, P.K. Bajpai, J. Mittal, C. Arora, Utilisation of cobalt doped Iron based MOF for enhanced removal and recovery of methylene blue dye from waste water, *J. Mol. Liq.*, 314 (2020) 113642, doi: 10.1016/j.molliq.2020.113642.
- [5] J. Mittal, Permissible synthetic food dyes in India, *Resonance-J. Sci. Educ.*, 25 (2020) 567–577.
- [6] A.K. Sharma, I. Singh, A rapid spectrophotometric method for trace determination of zinc, *Food. Anal. Method.*, 2 (2009) 311–316.
- [7] G.C. Ghosh, T.K. Chakraborty, S. Zaman, M.N. Nahar, A.H.M.E. Kabir, Removal of Methyl orange dye from aqueous solution by a low-cost activated carbon prepared from Mahagoni (*Swietenia mahagoni*) bark, *Environ. Pollut.*, 6 (2020) 171–184.
- [8] S.D. Richardson, C.S. Willson, K.A. Rusch, Use of rhodamine water tracer in the marshland upwelling system, *Ground Water*, 42 (2004) 678–688.
- [9] R. Ahmad, I. Hasan, A. Mittal, Adsorption of Cr(VI) and Cd(II) on chitosan grafted polyaniline-OMMT nanocomposite: isotherms, kinetics and thermodynamics studies, *Desal. Water Treat.*, 58 (2017) 144–153.
- [10] H.L. Wang, W. Zhi, N. Deng, G.D. Ji, Review on the fate and mechanism of nitrogen pollutant removal from wastewater using a biological filter, *Pol. J. Environ. Stud.*, 26 (2017) 1943–1954.
- [11] V. Kumar, P. Saharan, A.K. Sharma, A. Umar, I. Kaushal, A. Mittal, Y. Al-Hadeethi, B. Rashad, Silver doped manganese oxide-carbon nanotube nanocomposite for enhanced dye-sequestration: isotherm studies and RSM modelling approach, *Ceram. Int.*, 46 (2020) 10309–10319.
- [12] D. Liu, J.L. Yin, H. Tang, H. Wang, S.S. Liu, T.T. Huang, S.S. Fang, K.X. Zhu, Z.L. Xie, Fabrication of ZIF-67@PVDF ultrafiltration membrane with improved antifouling and separation performance for dye wastewater treatment via sulfate radical enhancement, *Sep. Purif. Technol.*, 279 (2021) 119775, doi: 10.1016/j.seppur.2021.119755.
- [13] R. Jain, P. Sharma, S. Sikarwar, J. Mittal, D. Pathak, Adsorption kinetics and thermodynamics of hazardous dye Tropaeoline 000 onto Aerioxide Alu C (Nano alumina): a non-carbon adsorbent, *Desal. Water Treat.*, 52 (2014) 7776–7783.
- [14] J. Mittal, A. Mariyam, F. Sakina, R.T. Baker, A.K. Sharma, A. Mittal, Batch and bulk adsorptive removal of anionic dye using metal/halide-free ordered mesoporous carbon as adsorbent, *J. Cleaner Prod.*, 321 (2021) 129060, doi: 10.1016/j.jclepro.2021.129060.
- [15] P. Saharan, V. Kumar, J. Mittal, V. Sharma, A.K. Sharma, Efficient ultrasonic assisted adsorption of organic pollutants employing bimetallic-carbon nanocomposites, *Sep. Sci. Technol.*, 56 (2020) 2895–2908.
- [16] I. Anastopoulos, I. Pashalidis, A.G. Orfanos, I.D. Manariotis, T. Tatarchuk, L. Sellaoui, A. Bonilla-Petriciolet, A. Mittal, A. Núñez-Delgado, Removal of caffeine, nicotine and amoxicillin from (waste)waters by various adsorbents. A review, *J. Environ. Manage.*, 261 (2020) 110236, doi: 10.1016/j.jenvman.2020.110236.
- [17] S.K. Sharma, In: *Hen Feather, A Remarkable Adsorbent for Dye Removal, Green Chemistry for Dyes Removal from Wastewater*, Scrivener Publishing LLC, USA, 2015, pp. 409–457.
- [18] F. Mahmoudi, M.M. Amini, M. Sillanpää, Hydrothermal synthesis of novel MIL-100(Fe)@SBA-15 composite material with high adsorption efficiency towards dye pollutants for wastewater remediation, *J. Taiwan Inst. Chem. Eng.*, 116 (2020) 303–313.
- [19] H. Daraei, A. Mittal, Investigation of adsorption performance of activated carbon prepared from waste tire for the removal of methylene blue dye from wastewater, *Desal. Water Treat.*, 90 (2017) 294–298.
- [20] C. Arora, P. Kumar, S. Soni, J. Mittal, A. Mittal, B. Singh, Efficient removal of malachite green dye from aqueous solution using

- Curcuma caesia* based activated carbon, Desal. Water Treat., 195 (2020) 341–352.
- [21] B.K. Selvan, K. Thiagarajan, S. Das, N. Jaya, S.A. Jabasingh, P. Saravanan, M. Rajasimman, Y. Vasseghian, Synthesis and characterization of nano zerovalent iron-kaolin clay (nZVI-Kaol) composite polyethersulfone (PES) membrane for the efficacious As_2O_3 removal from potable water samples, Chemosphere., 288 (2021) 132405, doi: 10.1016/j.chemosphere.2021.132405.
- [22] W.B. Yang, Y.Q. Lu, F.F. Zheng, X.X. Xue, N. Li, D.M. Liu, Adsorption behavior and mechanisms of norfloxacin onto porous resins and carbon nanotube, Chem. Eng. J., 179 (2012) 112–118.
- [23] S. Soni, P.K. Bajpai, D. Bharti, J. Mittal, C. Arora, Removal of crystal violet from aqueous solution using iron based metal organic framework, Desal. Water Treat., 205 (2020) 386–399.
- [24] T. Somayeh, B. Alireza, A. Abolghasem, A. Nasrin, Adsorption of heavy metal ions from aqueous solutions using metal organic frameworks: kinetic and thermodynamic study, Desal. Water Treat., 162 (2019) 193–206.
- [25] B. Haddada, A. Mittal, J. Mittal, A. Paolone, D. Villemin, M. Debda, G. Mimanne, A. Habibi, Z. Hamidi, M. Boumediene, E. Belarbi, Synthesis and characterization of egg shell (ES) and egg shell with membrane (ESM) modified by ionic liquids, Chem. Data Collect., 33 (2021) 100717, doi: 10.1016/j.cdc.2021.100717.
- [26] A. Patel, S. Soni, J. Mittal, A. Mittal, C. Arora, Sequestration of crystal violet from aqueous solution using ash of black turmeric rhizome, Desal. Water Treat., 220 (2021) 342–352.
- [27] J. Mittal, R. Ahmad, A. Mariyam, V.K. Gupta, A. Mittal, Expedient and enhanced sequestration of heavy metal ions from aqueous environment by papaya peel carb and low-cost adsorbent, Desal. Water Treat., 210 (2021) 365–376.
- [28] C. Arora, D. Sahu, D. Bharti, V. Tamrakar, S. Soni, S. Sharma, Adsorption of hazardous dye crystal violet from industrial waste using low-cost adsorbent *Chenopodium album*, Desal. Water Treat., 167 (2019) 324–332.
- [29] C. Arora, P. Kumar, S. Soni, J. Mittal, A. Mittal, B. Singh, Efficient removal of malachite green dye from aqueous solution using *Curcuma caesia* based activated carbon, Desal. Water Treat., 195 (2020) 341–352.
- [30] J. Mittal, R. Ahmad, A. Mittal, Kahwa tea (*Camellia sinensis*) carbon-a novel and green low-cost adsorbent for the sequestration of Titan yellow dye from its aqueous solutions, Desal. Water Treat., 227 (2021) 404–411.
- [31] P. Liu, D.J. Zhong, Y.L. Xu, N.B. Zhong, G.J. He, Co/Fe co-doped porous graphite carbon derived from metal organic framework for microelectrolysis-Fenton catalytic degradation of Rhodamine B, J. Environ. Chem. Eng., 9 (2021) 105924, doi: 10.1016/j.jece.2021.105924.
- [32] N. Yao, P. Li, Z. Zhou, R. Meng, G. Cheng, W. Luo, Nitrogen engineering on 3D dandelion-flower-like CoS_2 for high performance overall water splitting, Small, 15 (2019) 1901993, doi: 10.1002/smll.201901993.
- [33] J. Balamurugan, S.G. Peera, M. Guo, T.T. Nguyen, N.H. Kim, J.H. Lee, A hierarchical 2D Ni–Mo–S nanosheet@nitrogen doped graphene hybrid as a Pt-free cathode for high-performance dye sensitized solar cells and fuel cells, J. Mater. Chem. A, 5 (2017) 17896–17908.
- [34] A.K. Sharma, Y. Sharma, p-toluene sulfonic acid doped polyaniline carbon nanotube composites: synthesis via different routes and modified properties, J. Electrochem. Sci. Eng., 3 (2013) 47–56.
- [35] S. Irfana, Z. Zhuanghao, F. Li, Y.X. Chena, G.-X. Liang, J.T. Luo, F. Ping, Critical review: bismuth ferrite as an emerging visible light active nanostructured photocatalyst, J. Mater. Res. Technol., 8 (2019) 6375–6389.
- [36] N. Ranga, E. Poonia, S. Jaxhar, A.K. Sharma, A. Kumar, S. Devi, S. Duhan, Enhanced antimicrobial properties of bioactive glass using strontium and silver oxide nanocomposites, J. Asian Ceram. Soc., 7 (2019) 75–81.
- [37] M. Teotia, A. Mittal, R.K. Soni, Chapter 3 – Light-Mediated Thermoset Polymers, V. Grumezescu, A. Mihai Grumezescu, Eds., Materials for Biomedical Engineering: Thermoset and Thermoplastic Polymers, Elsevier, Amsterdam, Netherlands, 2019, pp. 57–103.
- [38] R. Shanmugam, B. Jayaraman, V. Mohanraj, R.K. Ae, S. Sivaprakash, J.Y. Dong, Nitrogen-doped graphene encapsulated FeCoMoS nanoparticles as advanced trifunctional catalyst for water splitting devices and zinc-air batteries, Appl. Catal., B, 279 (2020) 119381, doi: 10.1016/j.apcatb.2020.119381.
- [39] J.X. Yu, J. Zhu, L.Y. Feng, X.L. Cai, Y.F. Zhang, R.A. Chi, Removal of cationic dyes by modified waste biosorbent under continuous model: competitive adsorption and kinetics, Arabian J. Chem., 12 (2019) 2044–2051.
- [40] N. Minju, K.V. Swaroop, K. Haribabu, V. Sivasubramanian, P.S. Kumar, Removal of fluoride from aqueous media by magnesium oxide-coated nanoparticles, Desal. Water Treat., 53 (2015) 2905–2910.
- [41] V.K. Gupta, S. Agarwa, L. Ahmad, A. Mirza, J. Mittal, Sequestration of toxic congo red dye from aqueous solution using ecofriendly guar/activated carbon nanocomposites, Int. J. Biol. Macromol., 158 (2020) 1310–1318.
- [42] A. Mariyam, J. Mittal, F. Sakina, R.T. Baker, A.K. Sharma, Fixed-bed adsorption of the dye Chrysoidine R on ordered mesoporous carbon, Desal. Water Treat., 229 (2021) 395–402.
- [43] J. Mittal, R. Ahmad, M.O. Ejaz, A. Mariyam, A. Mittal, A novel, eco-friendly bio-nanocomposites (Alg-Cst/Kal) for the adsorptive removal of crystal violet dye from its aqueous solutions, Int. J. Phytoremediation, 23 (2021) 1–13.
- [44] Y. Xiong, C. Zhang, M. Duan, J. Chen, S.W. Fang, J. Li, P. Shi, J.T. Ren, H.Q. Wan, Insight into organic pollutant adsorption characteristics on a g- C_3N_4 surface by attenuated total reflection spectroscopy and molecular dynamics simulation, Langmuir, 37 (2021) 7655–7667.
- [45] E. Abedi, M.J. Amiri, M. Sayadi, The potential use of ultrasound-assisted bleaching in removing heavy metals and pigments from soybean oil using kinetic, thermodynamic and equilibrium modeling, Environ. Sci. Pollut. Res., 28 (2021) 49833–49851.
- [46] V. Hoang Nguyen, D.T. Nguyen, T. Tung Nguyen, H. Phuong, T. Nguyen, H. Binh Khuat, T. Hung Nguyen, V. Khanh Tran, S. Woong Chang, P. Nguyen-Tri, D. Duc Nguyen, D. Duong La, Activated carbon with ultrahigh surface area derived from sawdust biowaste for the removal of Rhodamine B in water, Environ. Technol. Innovation, 24 (2021) 101811, doi: 10.1016/j.eti.2021.101811.
- [47] Y.Q. Zhao, H. Yang, J.F. Sun, Y. Zhang, S.B. Xi, Enhanced adsorption of Rhodamine B on modified oil-based drill cutting ash: characterization, adsorption kinetics, and adsorption isotherm, ACS Omega, 6 (2021) 17086–17094.
- [48] I. Razan, A.I. Fayrouz, A.G. Mazen, H. Mohamad, Controlled growth and composition of multivariate metal-organic frameworks-199 via a reaction-diffusion process, Nano Res., 14 (2020) 423–431.
- [49] Z.J. Yang, G.F. Wu, C. Gan, G.M. Cai, J.Y. Zhang, H.B. Ji, Effective adsorption of arsenate, dyes and eugenol from aqueous solutions by cationic supramolecular gel materials, Colloids Surf., A, 616 (2021) 126238, doi: 10.1016/j.colsurfa.2021.126238.
- [50] R. Rubab, S. Ali, A.U. Rehman, S.A. Khan, A.M. Khan, Templated synthesis of NiO/SiO₂ nanocomposite for dye removal applications: adsorption kinetics and thermodynamic properties, Colloids Surf., A, 615 (2021) 126253, doi: 10.1016/j.colsurfa.2021.126253.
- [51] H.X. Guo, F. Lin, J.H. Chen, F.M. Li, W. Weng, Metal-organic framework MIL-125(Ti) for efficient adsorptive removal of Rhodamine B from aqueous solution, Appl. Organomet. Chem., 29 (2015) 12–19.
- [52] I. Rabani, R. Zafar, K. Subalakshmi, H.-S. Kim, C. Bathula, Y.-S. Seo, A facile mechanochemical preparation of $Co_3O_4@g-C_3N_4$ for application in supercapacitors and degradation of pollutants in water, J. Hazard. Mater., 407 (2021) 124360, doi: 10.1016/j.jhazmat.2020.124360.
- [53] C. Yang, G.H. Zhang, Y. Meng, G.X. Pan, Z.M. Ni, S.J. Xia, Direct Z-scheme $CeO_2@LDH$ core-shell heterostructure for photodegradation of Rhodamine B by synergistic persulfate

- activation, *J. Hazard. Mater.*, 408 (2021) 124908, doi: 10.1016/j.jhazmat.2020.124908.
- [54] Z.J. Huang, Z. Lai, D.Y. Zhu, H.Y. Wang, C.X. Zhao, G.H. Ruan, F.Y. Du, Electrospun graphene oxide/MIL-101(Fe)/poly(acrylonitrile-co-maleic acid) nanofiber: a high-efficient and reusable integrated photocatalytic adsorbents for removal of dye pollutant from water samples, *J. Colloid Interface Sci.*, 597 (2021) 196–205.
- [55] R. Jain, M. Mathur, S. Sikarwar, A. Mittal, Removal of the hazardous dye Rhodamine B through photocatalytic and adsorption treatments, *J. Environ. Manage.*, 85 (2007) 956–964.
- [56] A. Mariyam, J. Mittal, F. Sakina, R.T. Baker, A.K. Sharma, Adsorption behaviour of Chrysoidine R dye on a metal/halide-free variant of ordered mesoporous carbon, *Desal. Water Treat.*, 223 (2021) 425–433.
- [57] A. Mariyam, J. Mittal, F. Sakina, R.T. Baker, A.K. Sharma, A. Mittal, Efficient batch and fixed-bed sequestration of a basic dye using a novel variant of ordered mesoporous carbon as adsorbent, *Arabian J. Chem.*, 14 (2021) 103186, doi: 10.1016/j.arabjc.2021.103186.
- [58] L. Labiadh, A.R. Kamali, 3D graphene nanoedges as efficient dye adsorbents with ultra-high thermal regeneration performance, *Appl. Surf. Sci.*, 490 (2019) 383–394.
- [59] Y. Zhang, N.A. Liu, Y. Yang, J. Li, S. Wang, J. Lv, R. Tang, Novel carbothermal synthesis of Fe, N co-doped oak wood biochar (Fe/N-OB) for fast and effective Cr(VI) removal, *Colloids Surf., A*, 600 (2020) 124926, doi: 10.1016/j.colsurfa.2020.124926.
- [60] B. Pourgolmohammad, S.M. Masoudpanah, M.R. Aboutalebi, Synthesis of CoFe_2O_4 powders with high surface area by solution combustion method: effect of fuel content and cobalt precursor, *Ceram. Int.*, 43 (2017) 3797–3803.
- [61] Y. Xie, X. Yuan, Z. Wu, G. Zeng, L. Jiang, X. Peng, H. Li, Adsorption behavior and mechanism of Mg/Fe layered double hydroxide with Fe_3O_4 -carbon spheres on the removal of Pb(II) and Cu(II), *J. Colloid Interface Sci.*, 536 (2019) 440–455.
- [62] H.J. Su, Z.Q. Fang, P.E. Tsang, J.Z. Fang, D.Y. Zhao, Stabilisation of nanoscale zero-valent iron with biochar for enhanced transport and in-situ remediation of hexavalent chromium in soil, *Environ. Pollut.*, 214 (2016) 94–100.
- [63] S. Keerthana, R. Yuvakkumar, G. Ravi, S. Pavithra, M. Thambidurai, C. Dang, D. Velauthapillai, Pure and Ce-doped spinel CuFe_2O_4 photocatalysts for efficient Rhodamine B degradation, *Environ. Res.*, 200 (2021) 111–528.
- [64] K. Atacan, N. Güy, M. Özcart, Design and synthesis of magnetically separable $\text{CuFe}_2\text{O}_4/\text{MoS}_2$ p-n heterojunction for photocatalytic efficiency of Rhodamine B degradation, *Colloid Interface Sci. Commun.*, 40 (2021) 100359, doi: 10.1016/j.colcom.2020.100359.
- [65] S. Samakchi, N. Chaibakhsh, Z. Moradi-Shoeili, Synthesis of $\text{MoS}_2/\text{MnFe}_2\text{O}_4$ nanocomposite with highly efficient catalytic performance in visible light photo-Fenton-like process, *J. Photochem. Photobiol., A*, 367 (2018) 420–428.
- [66] S. Xue, B. Tu, Z. Li, X. Ma, Y. Xu, M. Li, C. Fang, H. Tao, Enhanced adsorption of Rhodamine B over *Zoysia sinica* Hance-based carbon activated by ammonium chloride and sodium hydroxide treatments, *Colloid Surf., A*, 618 (2021) 126489, doi: 10.1016/j.colsurfa.2021.126489.